JOURNAL OF GEOPHYSICAL RESEARCH, VOL. 106, NO. A1, PAGES 127–139, JANUARY 1, 2001

Response of the upper atmosphere to auroral protons

M. Galand[1], T.J. Fuller-Rowell[2], and M.V. Codrescu[2]

Space Environment Center, National Oceanic and Atmospheric Administration, Boulder, Colorado

Abstract. A three-dimensional, time-dependent, coupled model of the thermosphere and ionosphere has been used to assess the influence of proton auroral precipitation on Earth's upper atmosphere. Statistical patterns of auroral electron and proton precipitation, derived from DMSP satellite observations, have been used to drive the model. Overall, electrons are the dominant particle energy source, with protons contributing $\sim$ 15% of the total energy. However, owing to the offset of the proton auroral oval toward dusk, in certain spatial regions protons can carry most of the energy. This is the case particularly at the equatorward edge of the dusk sector and at the poleward edge of the dawn sector of the auroral oval. The increase in Pedersen conductivity raises the average Joule heating by $\sim$ 10%, so raising the E and F region temperature by as much as 7%. The enhanced E region ionization also drives stronger neutral winds in the lower thermosphere through ion drag, which alters the temperature structure through transport, adiabatic heating, and adiabatic cooling. The neutral wind velocity modifications in the E region can reach 40% in some sectors. In addition, the upwelling of neutral gas raises the N_2/O ratio, depleting the F region and so reducing the ion-drag driven winds in this region. This study illustrates the modest yet significant impact of auroral proton precipitation on the upper atmosphere.

1. Introduction

In the auroral regions, precipitating electrons and ions are a major source of ionization of the atmospheric neutrals, which can locally exceed the ionization from the solar EUV and UV sources. As a consequence, particle precipitation enhances the electron and ion densities and the electrical conductances of the atmosphere [see, e.g., *Fuller-Rowell and Evans*, 1987; *Basu et al.*, 1987; *Rees*, 1989]. Additionally, it is crucial in studies of the electrodynamics of the high-latitude ionosphere to have an accurate conductance model. Such a model makes it possible to infer Birkeland currents and electric field patterns from magnetometer data [*Doyle et al.*, 1986; *Rich et al.*, 1987, 1991] or to estimate the Joule heating from particle and electric field measurements [*Richmond and Kamide*, 1988].

As a result, efforts have been made in the modeling of electrical conductances induced by particle precipitation [*Robinson et al.*, 1987; *Germany et al.*, 1994; *Rees et al.*, 1995; *Brekke and Moen*, 1993], and statistical patterns for electrical conductances have been derived in order to obtain a global picture of the effect of ionization sources in high-latitude regions [*Wallis and Budzinski*, 1981; *Reiff*, 1984; *Fuller-Rowell and Evans*, 1987; *Hardy et al.*, 1987]. Nevertheless, in all but one of these models, the only energetic particles considered as a source of ionization are electrons. *Fuller-Rowell and Evans* [1987], however, included the proton energy flux as part of the electron flux, treating protons as if they were electrons.

Recent studies, relying on incoherent scatter radar measurements and simultaneous satellite observations, have shown that at given locations and times, protons are the major source of ionization [*Basu et al.*, 1987; *Senior et al.*, 1987; *Lilensten and Galand*, 1998]. Moreover, using a global thermosphere-ionosphere model, *Galand et al.* [1999] has also emphasized the role played by protons on the ionospheric densities and the importance of considering protons separately as a source of ionization. However, it should be pointed out that the values taken in this previous study for the incident electron and proton fluxes are very large, though possible, and the spatial structure of the energy flux in the auroral ovals are assumed colocated and symmetric with respect to the noon-midnight magnetic meridian. In the present work, a more realistic model for the incident particle characteristics is used. Finally, *Senior* [1991] compared conductances derived from European Incoherent SCATter radar (EISCAT) data with a statisti-

[1]Now at Center for Space Physics, Boston University, Boston, Mass.

[2]Also at Cooperative Institute for Research in Environmental Sciences, University of Colorado, Boulder.

Paper number 2000JA002009.
0148-0227/01/2000JA002009$09.00

cal model of conductances obtained from precipitating electron characteristics measured by the polar-orbiting DMSP satellites [*Hardy et al.*, 1987]. She found that the EISCAT-derived conductances agree well with the DMSP model in the morning sector but are systematically larger than the model in the evening sector. She suggested that this difference is due to E region electron production by energetic ion precipitation, which occurs preferentially in the evening sector.

In order to further investigate the contribution of protons on electrical conductances, we have used the Air Force Research Laboratory's auroral statistical model derived from the polar-orbiting DMSP satellite data to define the incident electron and proton characteristics patterns. The magnetic activity considered in the present study is moderate (Kp=3). The effect of protons on electrical conductances is assessed by applying simplified relations to the electron statistical patterns [*Robinson et al.*, 1987] and to the proton statistical patterns [*Galand and Richmond*, 2000]. Finally, we undertake a more comprehensive study of the response of the upper atmosphere to proton precipitation, using the Coupled Thermosphere-Ionosphere Model (CTIM) [*Fuller-Rowell et al.*, 1996]. A parameterization of the electron and ion production rates induced by a proton beam is included in the model in order to take into account the contribution of proton precipitation as a source of ionization [*Galand et al.*, 1999].

2. Statistical Model of Particle Precipitation

The Defense Meteorological Satellite Program (DMSP) satellites have a sun-synchronous, circular, polar, low-altitude orbit. Their approximate altitude is 850 km. They carry curved plate electrostatic analyzers, which monitor the influx of ions and electrons into the upper atmosphere. These particle detectors look toward the local zenith and cover an energy range from $\sim$ 50 eV to 30 keV in 20 channels spaced at equal intervals in energy on a logarithmic scale [*Hardy et al.*, 1985; *Hardy et al.*, 1989]. All ions are assumed to be protons, as we have no ion composition information from the instruments. Such an assumption is good at high latitudes, except during extreme geomagnetic storm conditions. From these data, statistical studies have been completed to determine the average characteristics of the incident auroral electrons [*Hardy et al.*, 1985, 1987] and of the incident auroral protons [*Hardy et al.*, 1989, 1991] precipitating into the atmosphere. The inferred auroral model depends on the magnetic activity indexed by Kp.

Where appropriate, the particle spectra were extrapolated up to 100 keV to compensate for the limitation in energy of the particle detectors. The extrapolation toward high energies is based on a Maxwellian distribution, which is a good approximation for electrons, but may tend to underestimate the high-energy tail of protons [*Lyons and Evans*, 1984; *Christon et al.*, 1991; *Decker et al.*, 1996; *Codrescu et al.*, 1997]. Moreover, auroral electron spectra usually follow a Maxwellian distribution in the keV energy range, covering the electron population responsible for most of the ionization. However, the low-energy part of the spectra typically increases with decreasing energy, departing from the Maxwellian distribution [*Robinson et al.*, 1987; *Meier et al.*, 1989]. This low-energy tail consists not only of the primary electrons but also of the secondary electrons produced by interaction of the primaries with the atmosphere. The low-energy electrons contribute little to the conductances. In order to obtain a reasonable Maxwellian fit to the important keV portion of the spectrum, the mean energy has to be calculated using the fluxes from a minimum energy $E^e_{\min}$ of 500 eV [*Robinson et al.*, 1987]. Since the electron mean energy patterns presented by *Hardy et al.* [1987] are associated with a minimum energy of 50 eV, they are not appropriate for the present study. We have derived the electron mean energy patterns by inverting the Pedersen conductance patterns proposed by *Hardy et al.* [1987]. These conductance patterns have been obtained by taking $E^e_{\min}$ equal to 500 eV to compute the electron mean energy. The inversion is based on the *Robinson et al.*'s [1987] formula defining the Pedersen conductance and discussed in section 3.

The statistical patterns of the energy flux and mean energy from DMSP are presented in Plates 1a and 1b, respectively, for electrons, and in Plates 1c and 1d, respectively, for protons. These patterns, valid for a moderate magnetic activity of Kp=3, are represented as polar spectrograms in the corrected geomagnetic latitude (CGL) [*Mayaud*, 1960; *Hakura*, 1965; *Gustafsson et al.*, 1992] and magnetic local time (MLT) coordinate system. The resolution of these patterns is half an hour in MLT and 1° in CGL between 60 and 80° and 2° in CGL between 50 and 60° and between 80 and 90°. The proton energy flux and mean energy patterns are from *Hardy et al.* [1989]. The electron energy flux pattern is determined in the same way as described by *Hardy et al.* [1987] but using the same years as those used for deriving the ion auroral model in order to insure consistency between the electron and ion patterns (D. Brautigam, personal communication, 1999). We have checked that considering a minimum energy of 50 or 500 eV does not make a significant difference in the values of the energy flux. As for the electron mean energy, the pattern is derived as explained above. Note that the particle patterns exhibit a clear asymmetry due to the eastward curvature gradient drift for electrons and the westward curvature gradient drift for protons from the midnight region [see, e.g., *Hargreaves*, 1992]. Moreover, the electron energy flux is an order of magnitude larger than that of protons on the nightside and 2 orders of magnitude larger in the morning sector. Nevertheless, as the electron and proton ovals are shifted, the addition of protons tends to broaden the width of the auro-

ral precipitation pattern, and the percentage of energy carried by protons can be larger than that of electrons for given times and locations. For instance, it reaches 100% at the equatorward boundary of the auroral oval before midnight, as illustrated in Plate 1e. In addition, in the cusp located around midday at magnetic latitudes higher than 75°, the protons carry almost 40% of the energy. In this region the electron mean energy has values less than 0.6 keV, and the electron energy flux is low. It should be noted that the energy flux and mean energy presented here are appropriate to a Maxwellian distribution in energy.

3. Statistical Model of Electrical Conductances

Prior to imposing the electron and proton sources on a sophisticated thermosphere-ionosphere model, it is instructive to estimate the Pedersen and Hall conductances using simplified relations. For electrons, we use the parameterization proposed by *Robinson et al.* [1987]:

$$\Sigma_P^e = \frac{40\,\langle E^e\rangle}{16+\langle E^e\rangle^2}\,\sqrt{Q_0^e} \qquad (1)$$

$$\Sigma_H^e = \frac{18\,\langle E^e\rangle^{1.85}}{16+\langle E^e\rangle^2}\,\sqrt{Q_0^e}, \qquad (2)$$

where the Pedersen and Hall conductances Σ_P^e and Σ_H^e induced by an incident electron beam are in Siemens, the electron incident energy flux Q_0^e is in mW m^{-2}, and the electron incident mean energy $\langle E^e\rangle$ is in keV, between 0.5 and 20. Equation (2) has been derived from *Robinson et al.*'s [1987] formulas (3) and (4).

This parameterization is derived from the work of *Vickrey et al.* [1981], using an energy deposition function to compute the ionization rate [*Rees*, 1963; *Berger et al.*, 1970] and adopting the effective mean recombination coefficient proposed by *Wickwar et al.* [1975], *Oran et al.* [1981], and *Vickrey et al.* [1982] to compute the electron density. The incident electron flux is assumed to be isotropic with a Maxwellian distribution in energy. The conductivities were computed using a standard model for the thermospheric state [*Banks and Kockarts*, 1973]. *Germany et al.* [1994] and *Rees et al.* [1995] calculated conductances that agree reasonably well with (1) and (2). *Germany et al.* [1994] also discussed the validity of using an effective recombination coefficient, comparing it against a full ion chemistry model. The latter predicts dependencies of the conductances on Q_0 with powers somewhat greater than 0.5, depending on the particle mean energy, owing to the fact that the dependence of the electron loss rate on electron density becomes less quadratic and more linear at higher altitudes, above 150 km.

For protons, we use the parameterization proposed by *Galand and Richmond* [2000]:

$$\Sigma_P^p = 5.7\,\sqrt{Q_0^p} \qquad (3)$$

$$\Sigma_H^p = 2.6\,\langle E^p\rangle^{0.3}\,\sqrt{Q_0^p}, \qquad (4)$$

where the Pedersen and Hall conductances Σ_P^p and Σ_H^p induced by an incident proton beam are in S, the proton incident energy flux Q_0^p is in mW m^{-2}, and the proton incident mean energy $\langle E^p\rangle$ is in keV, between 2 and 40.

This parameterization is derived from a proton transport code for computing the electron production rate [*Galand et al.*, 1997] and on the same effective mean recombination coefficient for deducing the electron density as used by *Robinson et al.* [1987]. The incident proton flux is assumed to be isotropic and to have a Maxwellian distribution in energy. The atmospheric neutral densities and temperatures are specified by the Mass Spectrometer and Incoherent Scatter model (MSIS-90) [*Hedin*, 1991] and the electron and ion temperatures, by the International Reference Ionosphere (IRI-90) [*Bilitza*, 1990]. The geomagnetic-field strength is obtained from the International Geomagnetic Reference Field model (IGRF-90) [*Langel*, 1992]. Finally, we choose to focus on the Northern Hemisphere, where the variation of the geomagnetic-field strength is relatively small. Therefore we have not included the dependence of the conductances on the geomagnetic-field strength discussed by *Galand and Richmond* [2000].

The parameterized Pedersen and Hall conductances induced by an incident particle beam of energy flux equal to 1 mW m^{-2} are plotted in Figure 1. As explained by *Galand and Richmond* [2000], the dependence of the conductances on mean energy is very different for electrons and protons. The Pedersen conductance, Σ_P^p, is independent, in first approximation, of the mean energy of the incident protons in the 2-40 keV range, whereas Σ_P^e depends significantly on the mean energy of the incident electrons. Moreover, for a given energy flux, Σ_P^p is always higher than Σ_P^e. For the Hall conductance, the comparison between electrons and protons depends not only on the incident energy flux but also on the incident mean energy. Note that for a given initial energy flux and a small electron mean energy, the Hall conductance induced by protons is always larger than that induced by electrons.

We have applied these simplified relations (1), (2), (3), and (4) to the patterns of the electron and proton characteristics presented in section 2 (Plate 1), in order to illustrate the conductances induced by auroral particles. Plates 2a and 2b show the Pedersen and Hall conductances induced by electron precipitation, for a magnetic activity of Kp=3. As discussed by *Galand and Richmond* [2000], the conductances induced by a combined electron-proton precipitation can be computed in applying a root-sum-square to the conductances induced by each particle type: $\Sigma^{e+p} = \sqrt{(\Sigma^e)^2 + (\Sigma^p)^2}$. The resulting Pedersen and Hall conductances are presented in Plates 2c and 2d, respectively. The addition of the proton contribution leads to an increase of the conductances, especially in the afternoon sector. Plates 2e and 2f show the percentage of increase of the conduc-

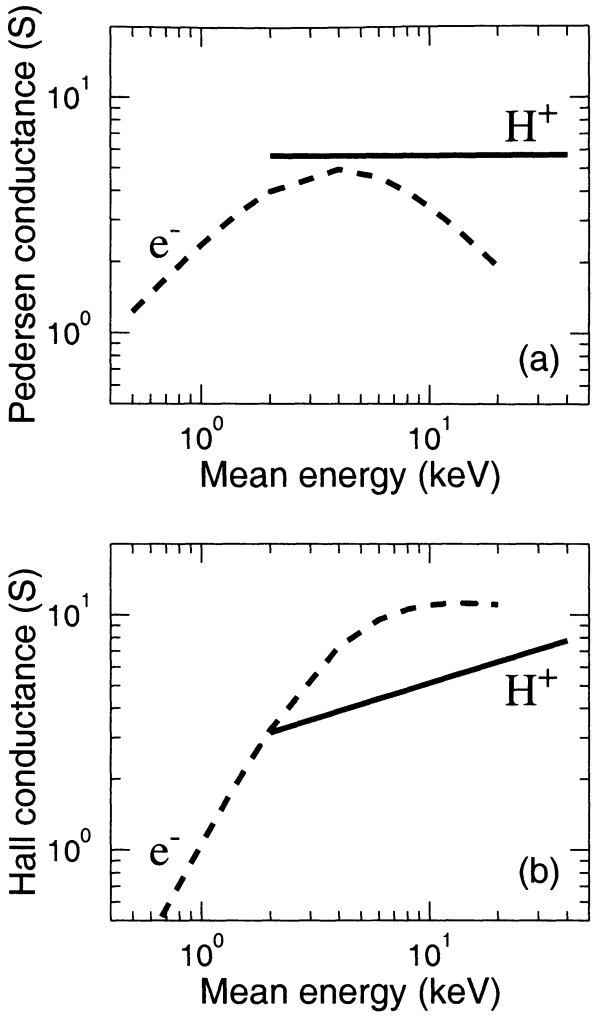

Figure 1. Electrical conductances induced by an incident particle flux, as a function of the mean energy $\langle E \rangle$ of the incident particles. The incident flux is assumed to have a Maxwellian distribution in energy and a normalized energy flux of 1 mW m^{-2}. Note that the mean energy $\langle E \rangle$ is equal to twice the characteristic energy E_0 of the incident particles. (a) Pedersen conductance Σ_P deduced from equation (1) for electrons (dashed line) and from equation (3) for protons (solid line). (b) Hall conductance Σ_H deduced from equation (2) for electrons (dashed line) and from equation (4) for protons (solid line).

tance resulting from the addition of the proton component when Σ^{e+p} is larger than 1 S. This increase is greater than 100% in the equatorward part of the auroral oval before midnight, a region where most of the energy is carried by protons (see Plate 1e). In this region, the absolute difference between Σ^{e+p} and Σ^e reaches a maximum of 3.8 S for Pedersen conductance and 4.3 S for Hall conductance. In addition, the proton contribution to conductances is sometimes significant in regions where protons do not carry most of the energy, such as the polar edge of the auroral oval around midday. This is a consequence of the large discrepancy between Σ^p and Σ^e when $\langle E^e \rangle$ is small, as illustrated in Figure 1. Thus, by adding protons, the Pedersen conductance in the cusp undergoes an increase larger than 100%. The enhancement of the Hall conductance is more spread in MLT due to the sharper decrease of Σ^e_H with decreasing energy compared with Σ^e_P (Figure 1). Nevertheless, we should point out that in these dayside regions the absolute values of the conductances are relatively small.

The large contribution of protons in the evening sector in the equatorward part of the auroral oval corroborates the earlier results from *Senior* [1991] who observed, in this region, larger values of conductances inferred from EISCAT compared with those determined from a model including only electron precipitation [*Hardy et al.*, 1987]. We also find a negligible effect of protons in the morning sector of the main auroral oval. A similar result was obtained by *Senior* [1991] and by *Watermann et al.* [1993] from incoherent scatter radar and satellite observations valid in the early morning dark auroral ionosphere.

4. Coupled Thermosphere-Ionosphere Model (CTIM)

The response of the upper atmosphere to auroral protons is examined by using the CTIM. This model is a three-dimensional, time-dependent model of Earth's upper atmosphere extending from 80 km up to ~ 500 km [*Fuller-Rowell et al.*, 1996]. The continuity, momentum, and thermodynamic equations are solved for the neutral gas and the plasma with a self-consistent aeronomic scheme for the coupled thermosphere and ionosphere system. The state equation of an ideal gas is applied and the equation of current density is solved. The global atmosphere is divided into a series of elements by geographic latitude, longitude, and pressure. Each grid point rotates with the Earth to define a noninertial frame of reference in a spherical polar coordinate system. The temporal resolution is 1 min. The latitude resolution is 2°; the longitude resolution is 18°. In the vertical direction the atmosphere is divided into 15 levels in logarithm of pressure from a lower boundary of 1 Pa at ~ 80 km altitude. The top pressure level at 8.6×10^{-7} Pa varies in altitude with changes in the temperature profile, between 300 km for very quiet magnetic conditions during solar minimum to 700 km for very disturbed magnetic conditions during solar maximum. In all cases, the range of pressure levels covers the ionospheric E and F regions.

The common input parameters of the global model are the solar EUV-UV spectral irradiance estimated from $F_{10.7}$, the auroral particle fluxes, the electric fields in high latitudes, the electron temperature profiles in altitude, and, at the lower altitude boundary, the upward propagating atmospheric tides. The model computes the density of the major constituents (N_2, O_2, and O) and the density of electrons and key ions (O^+, H^+, O_2^+, NO^+, N_2^+, and N^+). The neutral zonal, meridional, and

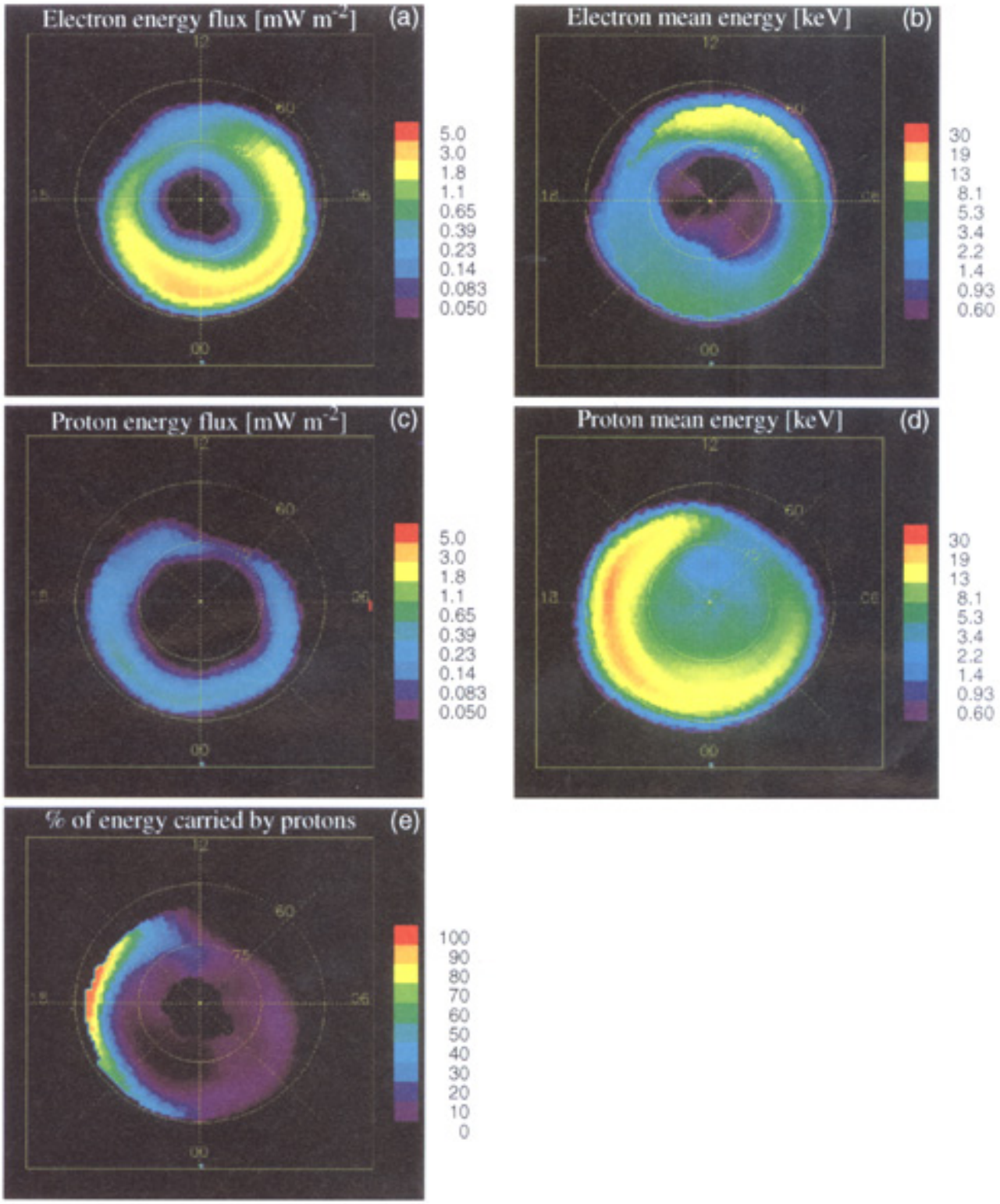

Plate 1. Polar view of the characteristics of incident particles for Kp=3 in a corrected geomagnetic latitude (CGL) and magnetic local time (MLT) coordinate system: (a) Electron energy flux in mW m^{-2}, (b) electron mean energy in keV, (c) proton energy flux in mW m^{-2}, (d) proton mean energy in keV, and (e) proportion of energy flux carried by protons in %. The perimeter in latitude is 50°. The percentage of energy carried by protons is plotted where the total energy flux is higher than 0.05 mW m^{-2}. The color scale is continuous. The values for some of the colors are given on the right side of each plot.

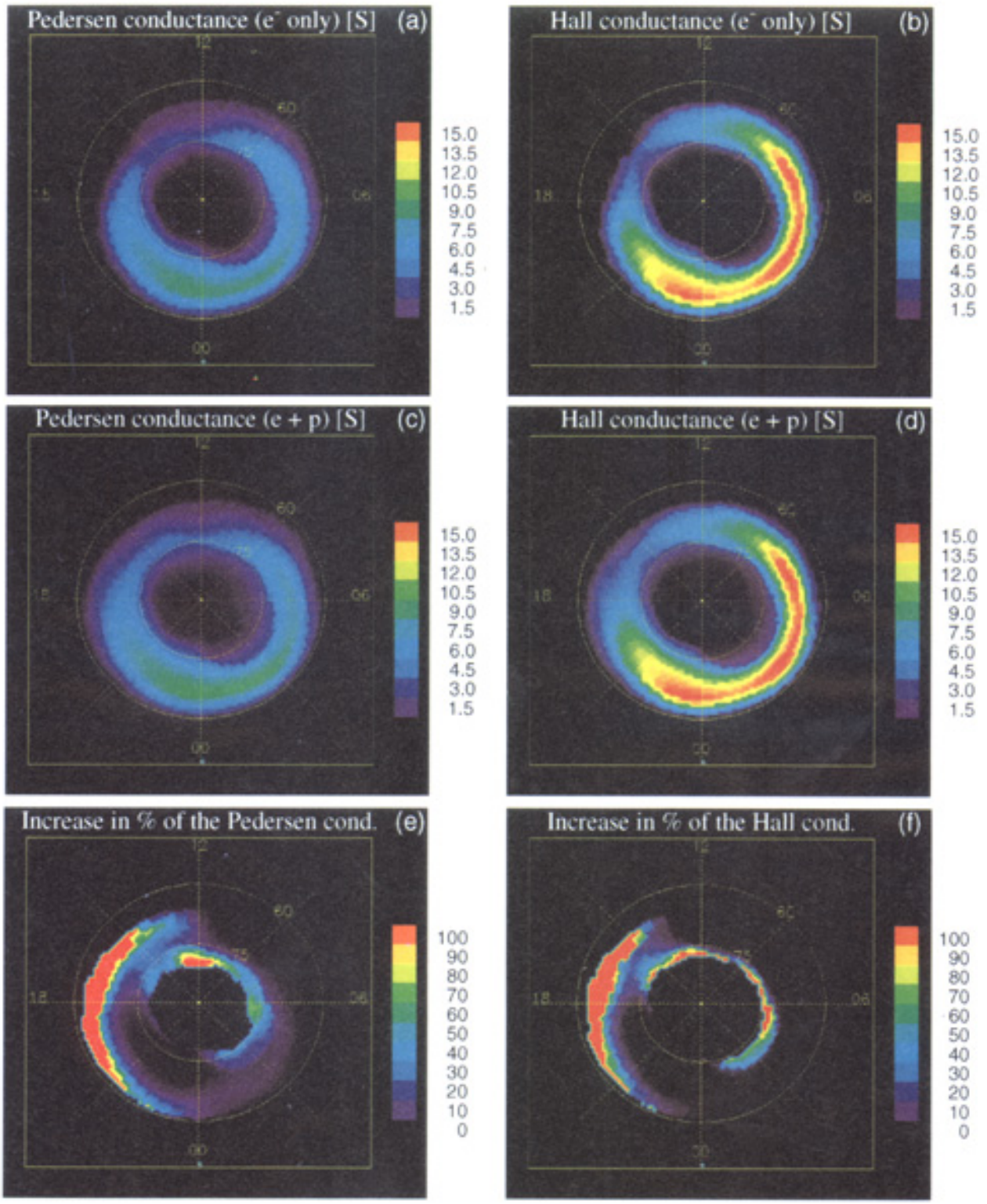

Plate 2. Polar view of the electrical conductances induced by energetic particles for Kp=3 and derived from equations (1), (2), (3), and (4), in a corrected geomagnetic latitude and magnetic local time coordinate system: (a) Pedersen conductance in S induced by electrons, (b) Hall conductance in S induced by electrons, (c) Pedersen conductance in S induced by combined electron and proton precipitation, (d) Hall conductance in S induced by combined electron and proton precipitation, (e) increase in percent of the Pedersen conductance resulting from taking the proton component into account, and (f) increase in percent of the Hall conductance resulting from taking the proton component into account. The perimeter in latitude is 50°. The color scale is continuous. The values for some of the colors are given on the right side of each plate.

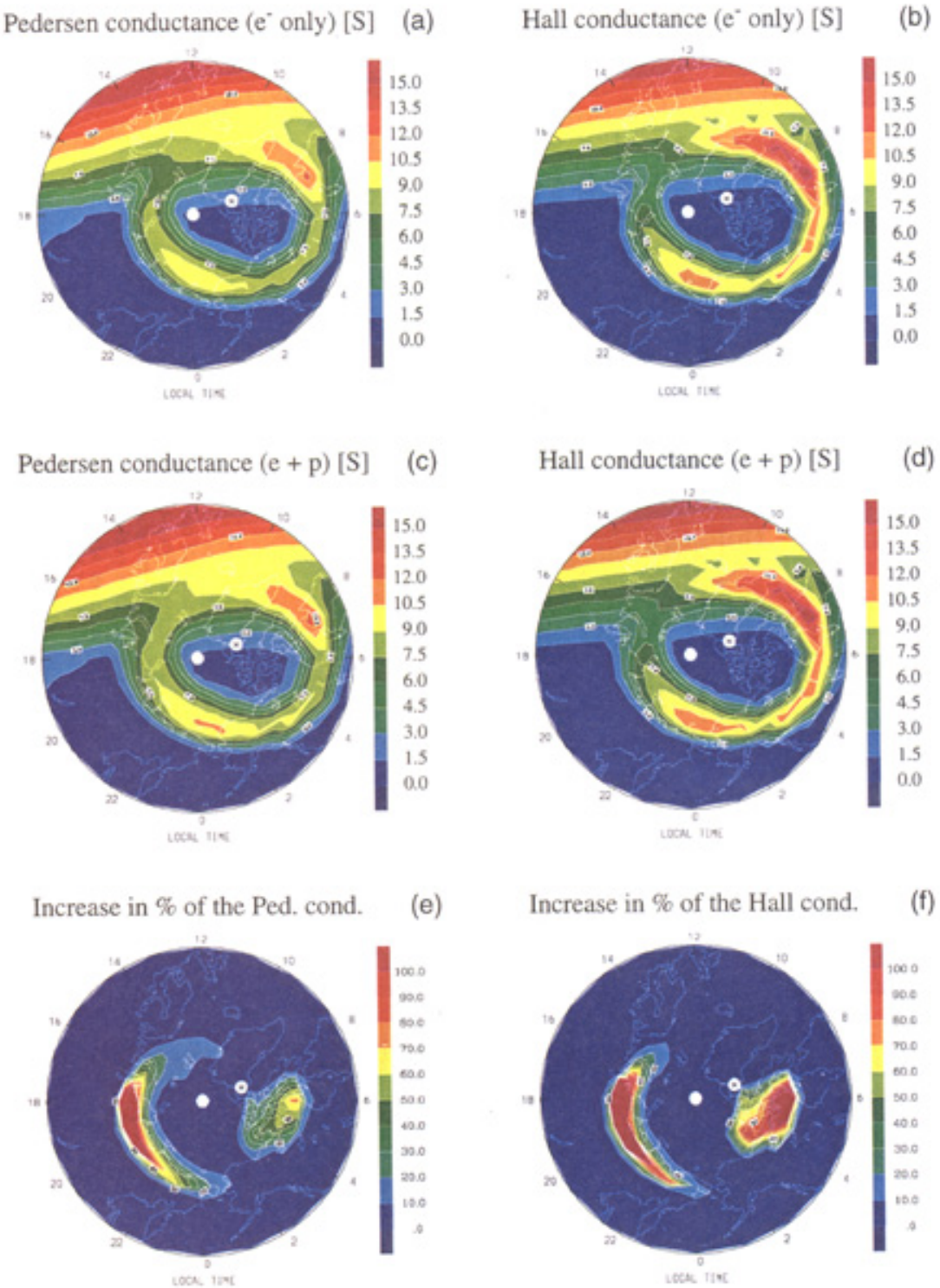

Plate 3. Polar view of the electrical conductances induced by energetic particles for Kp=3, at 1200 UT, and derived from CTIM, in a geographic latitude and local time coordinate system: (a) Pedersen conductance in S for case "e", (b) Hall conductance in S for case "e", (c) Pedersen conductance in S for case "e+p", (d) Hall conductance in S for case "e+p", (e) increase in percent of the Pedersen conductance resulting from including the proton component, and (f) increase in percent of the Hall conductance resulting from including the proton component. The perimeter in latitude is 50°. The scale for conductances is linear, from 0 to 15 S. The geographic pole is shown with a white circle, and the geomagnetic pole is shown with a cross in a white circle.

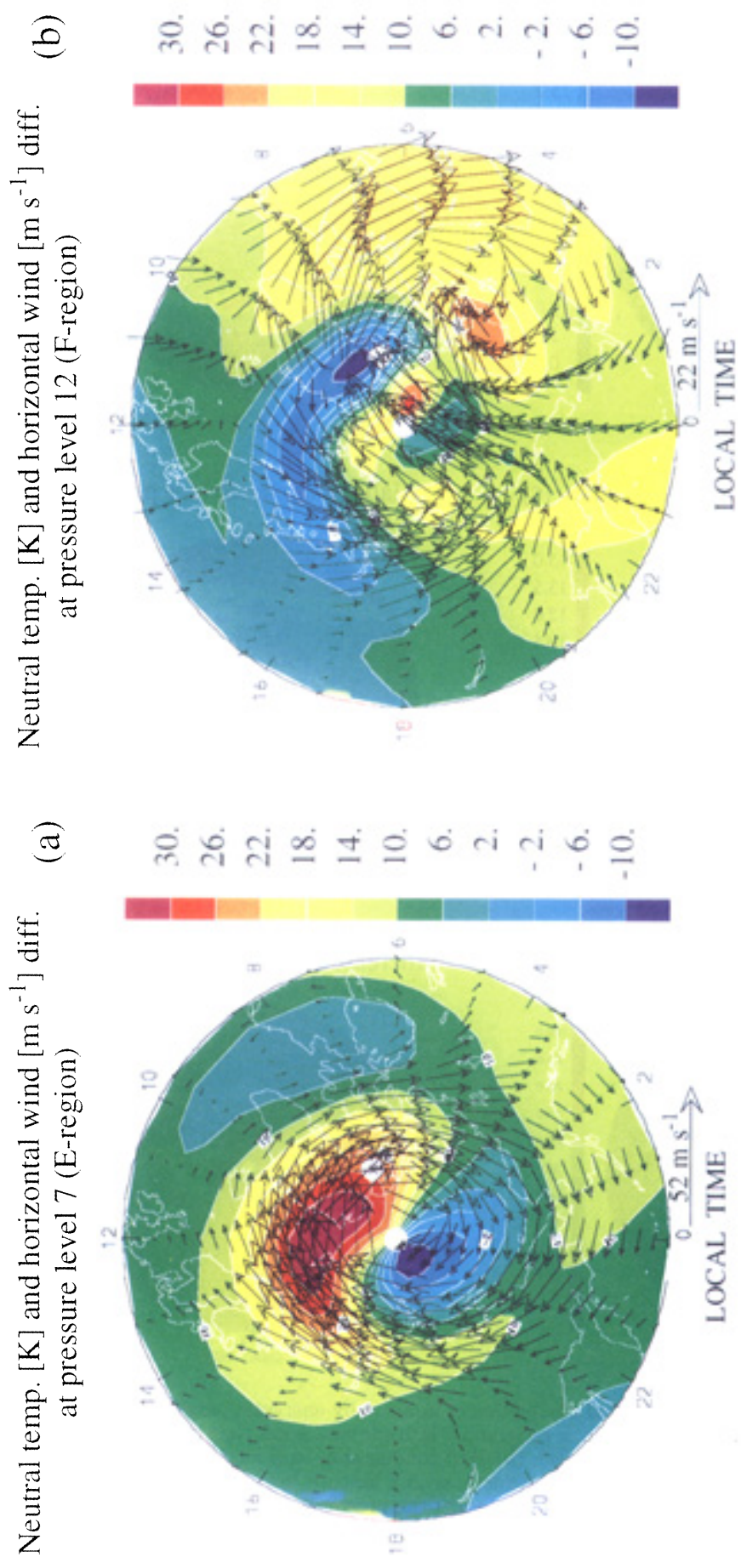

Plate 4. Polar view of the neutral temperature difference and neutral horizontal wind difference (case "e+p" minus case "e") for Kp=3, at 1200 UT, and derived from CTIM, in a geographic latitude and local time coordinate system: (a) for pressure level 7 corresponding to the E region, and (b) for pressure level 12 corresponding to the F region. The perimeter in latitude is 50°. The temperature differences are in K. The neutral wind differences are in m s^{-1}, and the arrow shown below each plot represents the maximum wind magnitude of 52 m s^{-1} for Plate 4a and of 22 m s^{-1} for Plate 4b. The geographic pole is shown with a white circle, and the geomagnetic pole is shown with a cross in a white circle.

vertical winds, the ion drift, and the ion and neutral temperatures are also computed, among other fields.

To take into account the auroral protons as a source of ionization, the parameterization of the electron and ion production rates from *Galand et al.* [1999] is included in the continuity equations of O^+, O_2^+, N_2^+, and N^+. This parameterization is valid for Maxwellian distribution in energy for the incident proton flux with mean energies between 2 and 40 keV. In addition, we assume the same neutral heating efficiency for proton precipitation as for electron precipitation [*Rees et al.*, 1983; *Rees*, 1987]. Starting from a base case valid for equinox and associated with a solar index $F_{10.7}$ of 160, we compare two simulations that have been performed until reaching steady state obtained after 3 simulated days: one including auroral electron precipitation (case "e") and the other including both auroral electron and proton precipitations (case "e+p"). The characteristics of the incident energetic particles are from the DMSP auroral statistical model discussed in section 2, for Kp=3 (see Plate 1).

Plates 3a and 3b for case "e" and Plates 3c and 3d for case "e+p" show the Pedersen conductance Σ_P and the Hall conductance Σ_H, respectively. The magnetic field model used in CTIM is based on an offset dipolar configuration. The conductances are presented as a polar view in a geographic latitude and a local time coordinate system for the Northern Hemisphere. Large conductance values are seen in the dayside due to the solar photon contribution and over the auroral ovals due to the energetic particle contribution. Proton precipitation, included in the model as a source of ionization, induces an increase of the density of electrons and of the major ions (O_2^+ and NO^+) in the E region [*Galand et al.*, 1999]. As a consequence, the electrical conductances as a function of the ion densities are increased in the auroral regions. The percentage increase induced by the proton precipitation is shown in Plates 3e and 3f for Σ_P and Σ_H, respectively. Note that around the geographic pole the conductances are not computed and the percentage increase is set to zero. As discussed in section 3, the proton contribution to conductances at a high latitude is large in regions where the percentage of energy flux carried by protons is high (region 1) (Plate 1e) or where the electron mean energy $\langle E^e \rangle$ is small (region 2) (Plate 1b). Region 1 is associated with the shift between the electron and proton auroral ovals explaining the crescent-like shape region of large conductance increase at the equatorward part of the auroral oval before midnight in Plates 3e and 3f. Both regions 1 and 2 contribute to the spot-like area in the morning sector associated with the polar edge of the auroral oval and to part of the polar cap, excluding the sunlit part (where the large photon-induced conductances mask the proton contribution). The spot-like area in Plates 3e and 3f corresponds to a region where Σ^{e+p} is relatively small, whereas the crescent-like area covers not only the equator edge of the auroral oval but also its center.

We have compared the conductances obtained from CTIM (Plate 3) with those derived from (1), (2), (3), and (4) which are valid for auroral electrons and protons (Plate 2). Since solar irradiance is also included in CTIM, this comparison can only be performed on the nightside. In both cases, the electron production rate associated with electron precipitation is based on the energy deposition function derived by *Rees* [1963]. In addition, the use of the parameterization for the electron and ion production rates for deriving the proton-induced conductances has been validated by *Galand and Richmond* [2000]. Moreover, the characteristics assumed for the energetic particles are the same as shown in Plate 1. Therefore we expect to find relatively good agreement between the simplified relations and the more comprehensive model. The regions of large proton contribution are, in fact, similar (compare Plates 2e to 3e and 2f to 3f). One has to keep in mind that Plates 2e and 2f are showing the percentage of increase only where the total conductance is larger than 1 S. Moreover, the Pedersen conductances have very close values (Plates 2a, 3a, 2c, and 3c). However, the Hall conductances shown in Plates 2b and 2d have values 25% larger than those presented in Plates 3b and 3d. The Hall conductivities are peaking below the Pedersen conductivities, between 110-120 km (see *Fuller-Rowell and Evans* [1987] for electron-induced conductivity profiles and *Galand and Richmond* [2000] for proton-induced conductivity profiles). In this region, the recombination coefficient for O_2^+ used in CTIM [*Fuller-Rowell*, 1993] compares well to the mean recombination coefficient used to derive the simplified relations discussed in section 3. However, that associated with NO^+ [*Fuller-Rowell*, 1993] is 40% higher than the mean recombination coefficient. Therefore, in CTIM, the loss rate is larger, inducing smaller electron density. This explains why we find lower values for the Hall conductance derived from CTIM compared with the case where the simplified relations are used.

Next we have estimated the Joule heating, a quantity representative of the thermal energy given to neutrals through collisions with ions which have been accelerated by the perpendicular electric field [*Fuller-Rowell et al.*, 1997]. The Joule heating is deduced from the electric field, the Pedersen conductance, and the neutral wind. Figure 2 shows hourly values of the northern hemispheric Joule heating for case "e" and case "e+p". The diurnal variation observed in the Joule heating in Figure 2 is due to the offset between the geographic pole and the geomagnetic pole. The maximum in Joule heating occurs when the area of the auroral oval illuminated by the sun is the largest, that is, when the magnetic pole is located at 12 local time. In Figure 2 the maximum is around 1700 UT, which is consistent with a longitude of the northern magnetic pole close to 80° west. Adding the proton precipitation associated with Kp=3 in the model induced an 8 GigaWatts (GW) increase in the Joule heating or 7 - 11%. We note that if the source is described as a constant electric current, an

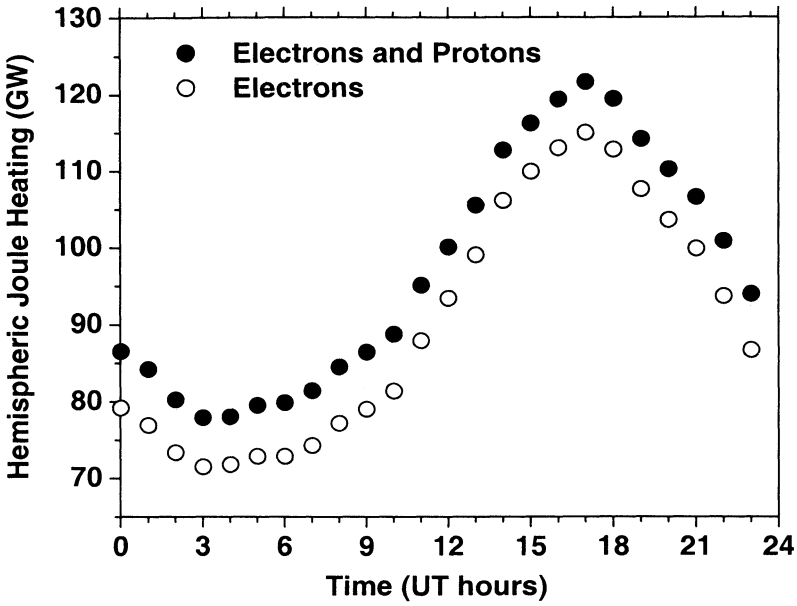

Figure 2. Hemispheric Joule heating for the Northern Hemisphere inferred from CTIM, as a function of universal time (UT). Case "e" is represented with open circle, and case "e+p" is represented with filled circles.

enhancement of the conductances induces a decrease of the electric field and therefore a decrease of the Joule heating. However, the high-latitude electric field used in this study is based on the model derived from Millstone Hill incoherent scatter observations and is assumed to be unchanged for the two simulations. This assumption implies a constant voltage source. Given these assumptions it is legitimate to infer that adding the proton contribution causes an increase in Joule heating.

Plate 4 shows the difference in neutral wind and temperature between case "e" (electrons only) and case "e+p" (electrons and protons). Plate 4a corresponds to a pressure level in the E region near 120 km, and Plate 4b corresponds to a pressure level in the F region near 300 km. Adding energetic protons enhances the Joule heating and the direct neutral heating (through chemistry), mainly in the E region where protons deposit most of their energy. This heating yields an increase of the neutral temperature in the auroral E region, especially at the equatorward edge of the oval before midnight. Owing to neutral winds blowing westward in the evening auroral zone, the heated neutrals are transported toward the dayside, where the largest increase of neutral temperature is seen. This increase is also induced by the convergence of the horizontal wind, which tends to be balanced by a downward motion, leading to an adiabatic heating (see Plate 4). Adding proton precipitation in the model leads to an increase of up to 7% of the neutral temperature, which is significant given that solar diurnal and tidal modulations are $\sim$ 20%. In addition, with the higher conductances, the ion drag is increased, which drives higher neutral wind velocities, as illustrated in Plate 4a. The largest difference of neutral winds between case "e" and case "e+p" occurs in early afternoon and corresponds to an increase of 40%. As a result of the enhanced wind velocity, the dominant vortex associated with the horizontal wind in the afternoon sector [*Fuller-Rowell*, 1995] experiences less convergence. Therefore this vortex tends to open, and its center becomes cooler, as seen in Plate 4a. The increased neutral heating in the auroral E region induces an expansion of the upper thermosphere that produces horizontal pressure gradients and drives divergent winds. The divergence in the wind system drives upwelling which changes the neutral composition on pressure surfaces. The N_2 density is enhanced in the F region inducing more recombination and decreasing the electron and ion densities. Ion drag is therefore reduced, and the neutral winds are smaller by up to 8%. A reduction of westward winds in the afternoon sector is shown by the net eastward wind in the difference field of Plate 4b. As a result, there is redistribution of energy by the neutral field, resulting in a small decrease in the neutral temperature around 1200 local time (LT).

5. Conclusion

One of the highligths of the present study is the use of satellite observations to estimate the global ionosphere/thermosphere response to proton precipitation on the upper atmosphere. We have used the Air Force Research Laboratory's auroral statistical model derived from DMSP satellite data to define the characteristics of the incident energetic particles. While electrons are the dominant particle energy source at high latitudes, in some regions at certain times protons can carry most of the energy. This is the case at the equatorward edge of the auroral oval before midnight and in the cusp.

In addition, electrons and protons do not interact in the same way with the atmosphere. Therefore, even for smaller energy flux for protons compared with electrons, the response of the atmosphere to protons can be significant. Moreover, the proton spectra measured by DMSP have been extrapolated up to 100 keV assuming a Maxwellian distribution. If such a distribution fits reasonably well in the keV range, it may underestimate the high-energy tail [*Lyons and Evans*, 1984; *Hardy et al.*, 1987; *Christon et al.*, 1991; *Decker et al.*, 1996; *Codrescu et al.*, 1997]. Comprehensive studies need to be undertaken on a large number of spectra to get a better representation of the proton distribution over a wide range of energy.

In section 3 we have used simplified relations to illustrate electrical conductances caused by particle precipitation. Conductances have also been computed using the CTIM, as discussed in section 4. One of the interesting features of this global thermosphere-ionosphere model is its very good 2° resolution in latitude, which allows the shift of 3-5° between the electron and proton auroral ovals to be included. In order to take protons into account as a source of ionization, a parameterization of the electron and ion production rates induced by an incident proton beam was included in this global model. Conductances derived from (1), (2), (3), and (4) and conductances from CTIM have been compared for Kp=3, using the DMSP statistical model to define the characteristics of the incident particles. The comparison has been performed on the nightside where the only source of ionization is the particle precipitation. A very good agreement is obtained for the Pedersen conductances. For the Hall conductances the simplified relations provide values higher by 25% compared with CTIM values, apparently due to a difference in the recombination coefficients used. A large contribution of protons to electrical conductances is observed at the equatorward edge, and even the center part of the auroral oval before midnight, where protons carry a large fraction of the energy. This result confirms the study of *Senior* [1991], who found that electron precipitation could not explain alone the EISCAT-inferred conductances in the evening auroral sector. Note that in this region the total conductance has relatively high values. A large contribution of protons to conductances is also seen in regions where the electron mean energy $\langle E^e \rangle$ is very small. As pointed out above, electrons do not interact with the atmosphere in the same way as protons. For a given energy flux, proton-induced Pedersen conductance always has larger values than electron-induced conductance (Figure 2). Regions of low $\langle E^e \rangle$ and of a nonnegligible proton flux are the cusp, the polar edge of the auroral oval in the morning sector, and part of the polar cap. However, in these regions, particle-induced conductances have relatively small values. Note that when these regions with a large proton contribution undergo solar illumination, the proton influence on the total conductance is masked.

Using the CTIM, a more comprehensive study of the response of the upper atmosphere to proton precipitation has been undertaken (section 4). Under moderate conditions of Kp=3, auroral protons increase the hemispheric Joule heating by 8 GW or 10%. In addition, in the high-latitude noon and afternoon sectors, protons have significant effect on the neutral winds and temperatures of the E regions. In the F region the effect, even though noticeable, is smaller.

For moderately disturbed conditions (Kp=3), the proton contribution is relatively modest when integrated over the whole high-latitude region. However, locally or regionally, proton precipitation has a significant effect on the thermosphere and the ionosphere. For future studies it would be interesting to focus on more magnetically disturbed conditions.

Acknowledgments. We are indebted to D. Brautigam for providing us with the Air Force Research Laboratory statistical auroral particle model. We would like to thank him and F. Rich for their valuable comments on this model. We would like also to thank A. Richmond for very enriching discussions. In addition, we greatly appreciated the assistance from R. Viereck. M.G. gratefully acknowledges the financial support of the National Research Council and the NOAA Space Environment Center.

Janet G. Luhmann thanks the referees for their assistance in evaluating this paper.

References

Banks, P. M., and G. Kockarts, *Aeronomy*, Part A, Academic, San Diego, Calif., 1973.

Basu, B., J. R. Jasperse, R. M. Robinson, R. R. Vondrak, and D. S. Evans, Linear transport theory of auroral proton precipitation: A comparison with observations, *J. Geophys. Res.*, *92*, 5920-5932, 1987.

Berger, M. J., S. M. Seltzer, and K. Maeda, Energy deposition by auroral electrons in the atmosphere, *J. Atmos. Terr. Phys.*, *32*, 1015-1045, 1970.

Bilitza, D. (Ed.), *International Reference Ionosphere 1990*, *NSSDC 90-22*, Nat. Space Sci. Data Cent., Greenbelt, Md, 1990.

Brekke, A., and J. Moen, Observations of high latitude ionospheric conductances, *J. Atmos. Terr. Phys.*, *55*, 1493-1512, 1993.

Christon, S. P., D. J. Williams, D. G. Mitchell, C. Y. Huang, and L. A. Frank, Spectral characteristics of plasma sheet ion and electron populations during disturbed geomagnetic conditions, *J. Geophys. Res.*, *96*, 1-22, 1991.

Codrescu, M. V., T. J. Fuller-Rowell, R. G. Roble, and D. S. Evans, Medium energy particle precipitation influences on the mesosphere and lower thermosphere, *J. Geophys. Res.*, *102*, 19,977-19,987, 1997.

Decker, D. T., B. V. Kozelov, B. Basu, J. R. Jasperse, and V. E. Ivanov, Collisional degradation of the proton-H atom fluxes in the atmosphere: A comparison of theoretical techniques, *J. Geophys. Res.*, *101*, 26,947-26,960, 1996.

Doyle, M. A., W. J. Burke, D. A. Hardy, P. F. Bythrow, F. J. Rich, and T. A. Potemra, A simple model of auroral electrodynamics compared with HILAT measurements, *J. Geophys. Res.*, *91*, 6979-6985, 1986.

Fuller-Rowell, T. J., Modeling the solar cycle in nitric oxide in the thermosphere and upper mesosphere, *J. Geophys. Res.*, *98*, 1559-1570, 1993.

Fuller-Rowell, T. J., The dynamics of the lower thermo-

sphere, in *The Upper Mesosphere and Lower Thermosphere: A Review of Experiment and Theory, Geophys. Monogr. Ser.*, vol. 87, edited by R. M. Johnson and T. L. Killeen, pp 23-36, AGU, Washington, D.C., 1995.

Fuller-Rowell, T. J., and D. S. Evans, Height-integrated Pedersen and Hall conductivity patterns inferred from the TIROS-NOAA satellite data, *J. Geophys. Res.*, *92*, 7606-7618, 1987.

Fuller-Rowell, T. J., D. Rees, S. Quegan, R. J. Moffett, M. V. Codrescu, and G. H. Millward, A Coupled Thermosphere-Ionosphere Model (CTIM), in *Solar-Terrestrial Energy Program: Handbook of Ionospheric Models*, edited by R. W. Schunk, pp 217-238, Sol. Terr. Energy Prog., Logan, Ut., 1996.

Fuller-Rowell, T. J., M. V. Codrescu, R. G. Roble, and A. D. Richmond, How does the thermosphere and ionosphere react to a geomagnetic storm?, in *Magnetic Storms, Geophys. Monogr. Ser.*, vol. 98, edited by B.T. Tsurutani et al., pp 203-225, AGU, Washington, DC, 1997.

Galand, M., and A. D. Richmond, Ionospheric electrical conductances produced by auroral proton precipitation, *J. Geophys. Res.*, this issue, 2000.

Galand, M., J. Lilensten, W. Kofman, and R. B. Sidje, Proton transport model in the ionosphere, 1, Multistream approach of the transport equations, *J. Geophys. Res.*, *102*, 22,261-22,272, 1997.

Galand, M., R. Roble, and D. Lummerzheim, Ionization by energetic protons in Thermosphere-Ionosphere Electrodynamics - General Circulation Model, *J. Geophys. Res.*, *104*, 27,973-27,989, 1999.

Germany, G. A., D. G. Torr, P. G. Richards, M. R. Torr, and S. John, Determination of ionospheric conductivities from FUV auroral emissions, *J. Geophys. Res.*, *99*, 23,297-23,305, 1994.

Gustafsson, G., N. E. Papitashvili, and V. O. Papitashvili, A revised corrected geomagnetic coordinate system for epochs 1985 and 1990, *J. Atmos. Terr. Phys.*, *54*, 1609-1631, 1992.

Hakura, Y., Tables and maps of geomagnetic coordinates corrected by the higher order spherical harmonic terms, *Rep. Ionos. Space Res. Jpn*, *19*, 121-157, 1965.

Hardy, D. A., M. S. Gussenhoven, and E. Holeman, A statistical model of auroral electron precipitation, *J. Geophys. Res.*, *90*, 4229-4248, 1985.

Hardy, D. A., M. S. Gussenhoven, and R. Raistrick, Statistical and functional representations of the pattern of auroral energy flux, number flux, and conductivity, *J. Geophys. Res.*, *92*, 12,275-12,294, 1987.

Hardy, D. A., M. S. Gussenhoven, and D. Brautigam, A statistical model of auroral ion precipitation, *J. Geophys. Res.*, *94*, 370-392, 1989.

Hardy, D. A., W. McNeil, M. S. Gussenhoven, and D. Brautigam, A statistical model of auroral ion precipitation, 2, Functional representation of the average patterns, *J. Geophys. Res.*, *96*, 5539-5547, 1991.

Hargreaves, J. K., *The Solar-Terrestrial Environment*, Cambridge Univ. Press, New York, 1992.

Hedin, A. E., Extension of the MSIS thermosphere model into the middle and lower atmosphere, *J. Geophys. Res.*, *96*, 1159-1172, 1991.

Langel, R. A., International Geomagnetic Reference Field: The sixth generation, *J. Geomagn. Geoelectr.*, *44*, 679-707, 1992.

Lilensten, J., and M. Galand, Proton-electron precipitation effects on the electron production and density above EISCAT (Tromsø) and ESR, *Ann. Geophys.*, *16*, 1299-1307, 1998.

Lyons, L. R., and D. S. Evans, An association between discrete aurora and energetic particle boundaries, *J. Geophys. Res.*, *89*, 2395-2400, 1984.

Mayaud, P. N., Un nouveau système de coordonnées magnétiques pour l'étude de la haute atmosphère: les coordonnées de l'anneau équatorial, *Ann. Géophys.*, *278*, 278-288, 1960.

Meier, R. R., D. J. Strickland, J. H. Heicht, and A. B. Christensen, Deducing composition and incident electron spectra from ground-based auroral optical measurements: a study of auroral red line processes, *J. Geophys. Res.*, *94*, 13,541-13,552, 1989.

Oran, E. S., V. B. Wickwar, W. Kofman, and A. Newman, Auroral plasma lines: A first comparison of theory and experiment, *J. Geophys. Res.*, *86*, 199-205, 1981.

Rees, M. H., Auroral ionization and excitation by incident energetic electrons, *Planet. Space Sci.*, *11*, 1209-1218, 1963.

Rees, M. H., Modeling of the heating and ionizing of the polar thermosphere by magnetospheric electron and ion precipitation, *Phys. Scr. T.*, *T18*, 249-255, 1987.

Rees, M. H., *Physics and Chemistry of the Upper Atmosphere*, Cambridge Univ. Press, New York, 1989.

Rees, M. H., B. A. Emery, R. G. Roble, and K. Stamnes, Neutral and ion gas heating by auroral electron precipitation, *J. Geophys. Res.*, *88*, 6289-6300, 1983.

Rees, M. H., D. Lummerzheim, and R. G. Roble, Modeling of the atmosphere-magnetosphere-ionosphere system MAMI, *Space Sci. Rev.*, *71*, 691-703, 1995.

Reiff, P. H., Models of auroral-zone conductances, in *Magnetospheric Currents, Geophys. Monogr. Ser.*, vol. 28, edited by T. A. Potemra, pp. 180-191, AGU, Washington, D.C., 1984.

Rich, F. J., M. S. Gussenhoven, and M. E. Greenspan, Using simultaneous particle and field observations on a low altitude satellite to estimate Joule heat energy flow into the high latitude ionosphere, *Ann. Geophys.*, *6*, 527-534, 1987.

Rich, F. J., M. S. Gussenhoven, D. A. Hardy, and E. Holeman, Average height-integrated Joule heating rates and magnetic deflection vectors due to field-aligned currents during sunspot minimum, *J. Atmos. Terr. Phys.*, *53*, 293-308, 1991.

Richmond, A. D., and Y. Kamide, Mapping electrodynamics features of the high-latitude ionosphere from localized observations: Technique, *J. Geophys. Res.*, *93*, 5741-5759, 1988.

Robinson, R. M., R. R. Vondrak, K. Miller, T. Dabbs, and D. Hardy, On calculating ionospheric conductances from the flux and energy of precipitating electrons, *J. Geophys. Res.*, *92*, 2565-2569, 1987.

Senior, C., Solar and particle contributions to auroral height-integrated conductivities from EISCAT data: A statistical study, *Ann. Geophys.*, *9*, 449-460, 1991.

Senior C., J. R. Sharber, O. De La Beaujardière, R. A. Heelis, D. S. Evans, J. D. Winningham, M. Sugiura, and W. R. Hoegy, *E* and *F* region study of the evening sector auroral oval: A Chatanika/Dynamics Explorer 2/NOAA 6 comparison, *J. Geophys. Res.*, *92*, 2477-2494, 1987.

Vickrey, J. F., R. R. Vondrak, and S. J. Matthews, The diurnal and latitudinal variation of auroral zone ionospheric conductivity, *J. Geophys. Res.*, *86*, 65-75, 1981.

Vickrey, J. F., R. R. Vondrak, and S. J. Matthews, Energy deposition by precipitating particles and Joule dissipation in the auroral ionosphere, *J. Geophys. Res.*, *87*, 5184-5196, 1982.

Wallis, D. D., and E. E. Budzinski, Empirical models of height integrated conductivities, *J. Geophys. Res.*, *86*, 125-137, 1981.

Watermann, J., O. De La Beaujardière, and F. J. Rich, Comparison of ionospheric electrical conductances inferred from coincident radar and spacecraft measurements and photoionization models, *J. Atmos. Terr. Phys.*, *55*, 1513-1520, 1993.

Wickwar, V. B., M. J. Baron, and R. D. Sears, Auroral energy input from energetic electrons and Joule heating at Chatanika, *J. Geophys. Res.*, *80*, 4364-4367, 1975.

M. Galand, Center for Space Physics, Boston University, 725 Commonwealth Avenue, Boston, MA 02215. (mgaland@bu.edu)

M.V. Codrescu and T.J. Fuller-Rowell, Space Environment Center, National Oceanic and Atmospheric Administration, 325 Broadway, Boulder, CO 80303.

(Received February 18, 2000; revised March 21, 2000; accepted April 10, 2000.)